International Journal of
INTELLIGENT SYSTEMS AND APPLICATIONS IN ENGINEERING
ISSN:2147-6799 www.ijisae.org Original Research Paper

Optimal Deep Convolutional Neural Network Based Automated Brain Tumor Detection on MRI Multi-Modality Images

Sheethal M. S.*[1], Dr. P Amudha[2]

Submitted: 29/12/2023 **Revised**: 04/02/2024 **Accepted**: 12/02/2024

Abstract: Brain tumor (BT) detection utilizing magnetic resonance imaging (MRI) images has made significant progress by leveraging cutting-edge deep learning (DL) approaches. By developing the intricate designs and textures from the images, Convolutional Neural Networks (CNNs) are exposed to significant ability in accurately detecting tumor regions. These networks automatically learn important features in the MRI data, allowing them to differentiate among healthy brain tissue and abnormal regions indicative of tumors. By training on huge databases of annotated MRI images, these methods generalize well and identify tumors across different patient cases. The combination of CNNs with MRI-based tumor recognition not only improves diagnostic accuracy among them expedites the procedure, influences earlier strategies, and enhances patient outcomes. This manuscript offers the Optimal Deep Convolutional Neural Network Automated Brain Tumor Detection and Classification (ODCNN-ABTDC) technique on MRI multi-modality Images. The ODCNN-ABTDC technique mainly focused on the examination of brain MRI images for the classification and detection of BT. To accomplish this, the ODCNN-ABTDC technique involves a series of preprocessing steps to improve the quality of the image. In addition, the features from the preprocessed images are extracted by the use of grey level co-occurrence matrix. For the classification process, the ODCNN-ABTDC technique employs the CNN model which allocates the images into proper classes. Finally, the performance of the CNN model can be boosted by the Bayesian optimization (BO) algorithm. The experimental validation of the ODCNN-ABTDC technique is tested on the benchmark BRATS database. The extensive results demonstrated the greater solution of the ODCNN-ABTDC technique with other recent DL models.

Keywords: *Brain tumor, MRI Images, Multi-modality, Deep learning, Bayesian optimization, Convolutional neural network.*

1. Introduction

Brain tumor (BT) contains major threatening kinds of tumors worldwide. Glioma is the most popular early BT that takes place because of the carcinogenesis of glial cells in the brain and spinal cord [1]. Glioma is represented by numerous histological and cancerous grades and an average lifespan of less than 14 months after analysis for glioblastoma patients [2]. A common non-invasive approach is Magnetic Resonance Imaging (MRI), which generates a huge and different count of tissue variability in every imaging modality and is extensively utilized by medical experts for diagnosing BT [3]. However, the manual diagnosis and segmentation of structural MRI images of BT is a difficult and time-consuming activity, which can only be achieved by experienced neuro-radiologists. Classification BT is important and able to rescue patients [4]. An early and accurate analysis of a BT is significant for the patient's treatment procedure. However, the classification of tumors is a difficult and major challenge. Recently, physicians carried out considerable periods and work into creating breakthroughs for the classification of tumours in brain MRI images. Several approaches for attaining robust classification effectiveness are presented [5]. The majority of BT classification models have been still in the infancy of their observational data. Due to several causes like less tumor localization, insufficient training data, lower-quality image features, lower image quality, and others may affect the BT classification method [6].

The latest developments in machine learning (ML), especially in deep learning (DL) resulted in the detection and classification of medical imaging patterns [7]. Achievements in this field comprise the probability of recovering and extracting information from data rather than learning from scientific data or specialists. ML is quickly developing a useful tool for enhancing performance in several medical applications in different domains such as tissue segmentation, image classification, prognosis and analysis of diseases, and detection of cellular and molecular structures [8]. In image processing, highly effective methods are presently employed namely Convolutional Neural Networks (CNNs), as it has numerous layers and higher accurate diagnoses when the count of input images is great [9]. Autoencoders (AE) are an unsupervised learning approach that neural networks (NNs) can be leveraged for

[1] *Research Scholar, Department of Computer Science and Engineering, Avinashilingam Institute for home science and higher education for women, Coimbatore-641043.*
ORCID ID: 0000-0003-1196-7746
[2] *Professor, Department of Computer Science and Engineering, Avinashilingam Institute for home science and higher education for women, Coimbatore-641043..*
** Corresponding Author Email: sheethalbasil@gmail.com*

representation learning. Particularly, multiple DL and ML techniques are utilized for diagnosing cancers like lung cancer and identifying cardiovascular stenosis. Also, efficiency analyses are presented that can have higher diagnostic accuracy [10].

This manuscript offers the Optimal Deep Convolutional Neural Network Automated Brain Tumor Detection and Classification (ODCNN-ABTDC) technique on MRI multi-modality Images. The ODCNN-ABTDC technique involves a series of preprocessing steps to improve the quality of the image. In addition, the features from the preprocessed images are extracted by the use of a grey-level co-occurrence matrix (GLCM). For the classification process, the ODCNN-ABTDC technique employs the CNN model which allocates the images into proper classes. Finally, the performance of the CNN model can be boosted by the Bayesian optimization (BO) algorithm. The simulation value of the ODCNN-ABTDC technique is tested on the benchmark BRATS database.

2. Related Works

Saeedi et al. [11] developed 2 DL techniques and numerous ML methods for analyzing cancer. Firstly, preprocessing and augmentation algorithms are implemented. Secondly, the authors designed a novel 2D-CNN and a convolutional AE network. Next, 2D-CNN comprises many convolution layers and this network contains 8 convolutional and 4 pooling layers, and later each convolution layer, batch-normalization layers are utilized. In [12], the authors presented an IoT computational method that depends on DL for identifying BT in MRI images. This study developed integrating A CNN with LSTM; LSTMs increase the capability of CNN for extracting features. Saurav et al. [13] introduced a new lightweight attention-guided-CNN (AG-CNN) for BT classification in MRIs. This developed framework utilizes channel-attention blocks to concentrate on related areas of an image for classifying tumours.

Dipu et al. [14] introduced an automatic BT identification and segmentation approach, which is made by any DL-based object detection method. This technique employed seven various NN-based object detection models and approaches namely Scaled YOLO-V4, Detectron2, YOLO V5, Faster-RCNN, YOLO V4 Tiny, YOLO-V4 Darknet, and YOLO V3 Pytorch. In [15], a hybrid DL method CNN-LSTM to predict and classify BT through MRI was developed. Primarily, the data is effectively preprocessed and next, the CNN is implemented for extracting the important features from images. Harshavardhan et al. [16] suggested a Full Resolution Convolutional Network (FRCN) with an SVM algorithm for diagnosing tumors on MRI images. In the primary stage, the anisotropic filter can be employed for preprocessing raw MRI images, and then segmentation utilizing the SVM and skull classification. Eventually, the singular value decomposition and major element diagnosis processes can executed.

Turk et al. [17] recommended ensemble DL techniques (InceptionV3, VGG19, MobileNet, and ResNet-50) and Class Activation Maps (CAMs) approaches. This method employs 3-phases. Firstly, it is detected if it is a tumor in the MR images. Secondly, various kinds of tumors are diagnosed from MR images (Multiclass method). Lastly, CAMs for every tumor type are developed as the other tools for supporting the effort of physicians in tumor identification. In [18], an automated technique of BT classification depends on an improved DL method through DenseNet. The TL with the DenseNet121 algorithm is employed for classifying BT. The CNN technique can be optimized by hyper-parameters tuning the network.

3. The Proposed Model

In this manuscript, we have offered the development and design of the ODCNN-ABTDC method for the automated classification and identification of BT on MRI multi-modality Images. The ODCNN-ABTDC technique mainly focused on the examination of brain MRI images for the classification and recognition of BT. To accomplish this, the ODCNN-ABTDC technique involves several subprocesses namely preprocessing, GLCM feature extraction,

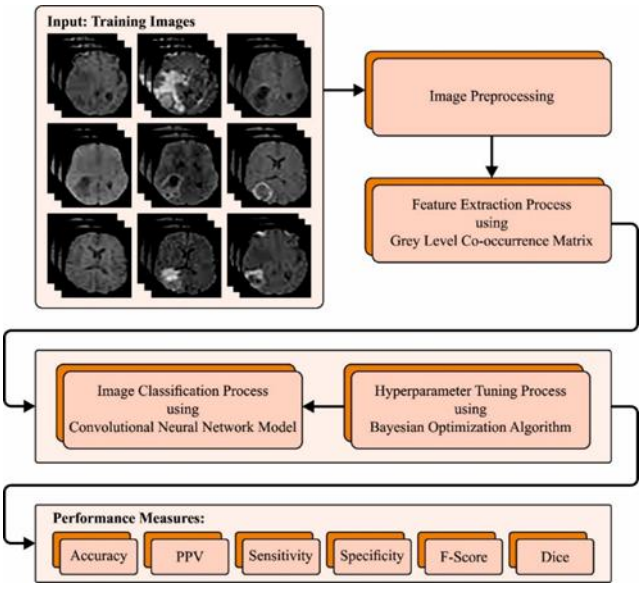

Fig. 1. Overall process of ODCNN-ABTDC algorithm

CNN-based classification, and BO-based hyperparameter tuning. Fig. 1 portrays the entire process of the ODCNN-ABTDC algorithm**.**

3.1. Image Preprocessing

In this study, the preprocessing of the input MRI images takes place in several stages:

Z-score Normalization: Z-score normalized is a method utilized for standardizing the intensity values of images. It contains subtracting the mean intensity in all the pixels and

then dividing by the standard deviation (SD). This procedure makes sure that the image intensity values take a mean of zero and SD of one, generating them equivalent and simpler to work with.

Skull Stripping using Edge Detection and Thresholding: Skull stripping is the procedure of eliminating the non-brain tissues in MRI images, leaving us one of the brain tissues for diagnosis. Edge detection systems are employed for identifying the edges of the brain, after that thresholding is executed for segmenting the brain in the rest of the images dependent upon intensity values. It supports isolating the brain region for detailed study.

Median Filtering (MF) and Bilateral Filtering (BF): MF is a nonlinear filter system that exchanges the pixel value with the median value of its adjacent pixels. It supports decreasing noise but maintaining edges from the image. BF is a difference of this that takes into account either spatial or intensity differences if executing the filter that supports noise decrease but preserves the entire design of the images.

Noise Removal using Mean and SD: Eliminating noise in the images filters out redundant differences in pixel values. Employing the mean and SD of whole images, you can execute filters to suppress pixel values that deviate considerably from the mean. It supports decreasing noise but maintaining the vital features of images.

Image Cropping and Resizing: During this case, the images can be resized to a size of 224x224 pixels. The resizing phase simplifies the following processing and analysis by making sure that every image takes similar sizes, helping the training and application of NN designs.

Data Augmentation: Data augmentation is a process utilized to artificially increase the training database by executing distinct transformations to new images. It is procedure supports diversifying the trained data, making the trained method more dependable and less prone to over-fit. Certain transformations contain scaling, flipping, and rotations. Scaling variations in the object sizes within them, rotations establish variability in the location of images, and flipping vertically or horizontally generates mirrored versions. By presenting these variations, the model learns to distinguish tumors regardless of their size, position, or orientation, resulting in enhanced generalized solutions on unseen data.

3.2. Feature Extraction using GLCM

To extract the features from the preprocessed images, the GLCM model is exploited. Generally, texture in an image depicts a repeating design of local variation from the intensity [19]. It offers data in the spatial arrangement of intensities or colours from the image, considered by the spatial distribution of intensity levels from the neighbourhood. During this process, consideration is provided to the connection among 2 pixels at a time is named as reference and neighbour pixel. This connection is portrayed in the procedure of co-occurrence matrix.

$$P_d[i,j] = n_{ij}. \tag{1}$$

Whereas, n_{ij} refers to the count of occurrences of the pixel values (i,j) posses at length d from the image. The occurrence matrix P_d is size nxn, whereas n signifies the amount of grey levels from the image. The grey levels from the image are detailed in quantization. The elements of P_d are then normalization employing the subsequent formula:

$$N[i,j] = \frac{P[i,j]}{\sum_{i=1}^{n} \quad \sum_{j=1}^{n} \quad P[i,j]}. \tag{2}$$

Through normalized, elements in matrix P_d take a value that ranges among 0 and 1, which permits it to be used as a probability function.

In GLCM, texture properties are captured. Utilizing a co-occurrence matrix, a feature vector is extracted in various methods. During this case, contrast is chosen in extracting the feature vector. The contrast is a measure of local variations existing from the image that is defined as:

$$C(k,n) = \sum_{i=1}^{n} \quad \sum_{j=1}^{n} \quad (i - j)^2 N[i,j]. \tag{3}$$

3.3. CNN-based Classification

For the BT detection process, the CNN approach can be employed. The architecture of DCNN includes FC, convolutional (Conv), and connected layers. Now, all the layers are used for implementing certain processes [20]. The main objective of Conv layer is to construct mapping features in binary pixel maps. Furthermore, the feature map produced was sub-sampled using the pooling function. The FC layer, in which video watermarking is implemented. Thus, Conv layer is well-ordered as multi-layer loops by successive Conv layers in deviation through the original Conv layer. The accuracy of the video watermarking process depends mainly on the quality of the DCNN layer. Fig. 2 demonstrates the architecture of CNN.

3.3.1 Conv layer: this layer is a connection of neurons, and Considers binary pixel maps as an input. Now, feature maps are formulated as and Conv neuron from a neighboring region considered neuron using trainable weight. Furthermore, Conv can be able to weight and input to create new feature maps. Later, Conv consequence is disseminated by a nonlinear activation function.

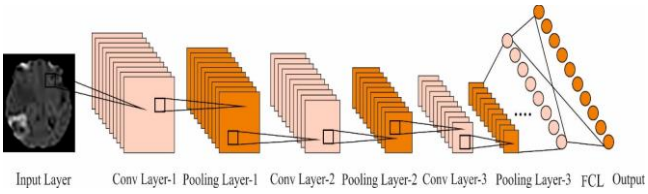

Fig. 2. CNN structure

$$Z = \{Z_1, Z_2, Z_3, \dots\dots, Z_n, .. Z_a\} \quad (4)$$

In Eq. (4), a shows the whole amount of Conv layers, Z_n indicates n^{th} Conv section in DCNN.

$$(Z_n^d)_{f,l} = (T_n^d)_{f,l} + \sum_{\psi=1}^{k_1^{n-1}} \sum_{m=-c_1^n}^{c_1^n} \sum_{v=-c_2^n}^{c_2^n} (\alpha_{d,\psi}^n)_{m,v} * (Z_n^{d-1})_{f+m,l+v} \quad (5)$$

In Eq. (5), $k_1{}^{n-1}$ denotes the whole feature map from previous Conv layer, $*$ shows Conv function, $(Z_n^d)_{f,l}, (Z_n^d)_{f,l}$ is fixed map from Conv layer, $\alpha_{d,\psi}^n \alpha_{d,\psi}^n$ indicates the kernel function, and $T_n^d T_n^d$ refers to bias.

3.3.2 Pooling layer: The Conv network realizes global pooling and local layer for minimizing computational process. The pooling component shrinkage data size by collaborating neuron cluster outcome at a single layer to one neuron from the resulting layer. The mapping feature was reduced to enhance feature invariance to variations existing in input since the pooling layer carries out a sub-sampling procedure.

3.3.3 FC layers: The feature in the Conv layer is exposed to the FC layer for the video watermarking process.

$$N_n^d = (G_n^d)$$

with

$$G_n^d = \sum_{\psi=1}^{k_1^{n-1}} \sum_{m=-c_1^n}^{c_1^n} \sum_{v=-c_2^n}^{c_2^n} (\alpha_{d,\psi}^n)_{m,v} * (Z_n^{d-1})_{f+m,l+v} \quad (6)$$

In Eq. (6), $(\alpha_{d,\psi}^n)_{m,v}$ denotes the weight connection component at (f, l) in ψ^{th} mapping feature of layer $(n\text{-}1)$ and d^{th} component in a layer in n.

Moreover, the activation layer can be used to generate pixel maps, and ReLU is regarded as an activation function to abolish negative standards that assurances easiness and efficiency in larger networks. The n^{th} nonlinear layer with feature map and outcome from the ReLu layer is given below,

$$Z_n^d = fun(Z_n^{d-1}) \quad (7)$$

In Eq. (7), fun () shows the activation process in $the\ n^{th}$ Conv layer. Moreover, the weight and bias existing in DCNN are optimally trained. M_k represents the binary pixel maps obtained as output from DCNN.

3.4. BO-based Hyperparameter Tuning

Finally, the hyperparameter tuning of the CNN approach takes place using the BO algorithm. Hyperparameter tuning is the core concept in machine learning, and before the model is trained, its setting can be resolved. Satisfying performance of the ML algorithm depends on proper hyperparameter settings [21]. Manual parameter tuning is uncertain and complicated, and the value of the hyperparameter has a direct impact on the predictive outcome of the model. BO finds a good combination of hyperparameters by using the Bayesian inference method and constructing a probabilistic model and realizes automatic and fast optimization of hyperparameters. Thus, the study uses BO for the hyperparameter of three categories of weak learners, to further increase the predictive outcome and generalization capability of the ensemble learning model, and effectively reduce the time and energy input of parameter tuning.

BO considers that there is a functional correlation between the loss function and the hyperparameter to be improved and that this functional correlation is a "black box function" that estimates the posterior distribution of the unknown objective function through the previous sample point. A set of hyperparameters is established that this result in a globally optimum solution by learning the shape of the objective function. BO is an approximation technique that uses a proxy function to fit the relationship between model evaluation and hyperparameters and then chooses a better combination of hyperparameters.

BO builds a probability model for the f function to be adjusted for the hyperparameter optimization problems of the XGBoost model, further exploits the model to select the next assessment point, and successively iterates to attain the optimum solution:

$$x^* = argminx_{x \in \chi \subseteq R^d} f(x) \quad (8)$$

In Eq. (8), λi indicates the decision space, x^* denotes the best hyperparameter combination, and $f(x)$ represents the objective function. The major step of the BO consists of the prior function and learning function.

3.4.1 Gaussian regression Process

The Gaussian model is a set of random variables and is a non-parametric model defined by the mean and the kernel functions as:

$$f(x) \sim gp\big(m(x), k(x, x')\big) \quad (9)$$

$$\{m(x) = E\big(m(x), k(x,x')\big)\, k(x,x') = E\big[\big(f(x) - m(x)\big)\big(f(x') - m(x')\big)\big] \quad (10)$$

Sample dataset $D = (x, y)$ of hyperparameter is constructed, where $X = (x_1, x_2, x_t)$ refers to the training set, $y = \{f(x_1), f(x_2), \ldots, f(x_t)\}$ denotes the set of (x):

$$[f(x_1)\ f(x_2)\ M\ f(x_t)\ ]: N(0, [k(x_1,x_1)\ \ldots\ k(x_1,x_t)\ \vdots \ddots \vdots\ k(x_t,x_1)\ \ldots\ k(x_t,x_t)\ ]) \quad (11)$$

If a new sample $Xt + 1$ is added and the covariance matrix, represented as K, is updated as:

$$[f_{1:t}\ f_{t+1}\ ] - N(0, K\ K\ k^T\ k(x_{t+1}, x_{t+1})\ ) \quad (12)$$

$$\{f_{1:t} = [f_1, f_2, \cdots f_t]^T\ k = [k(x_{t+1}, x_1), k(x_{t+1}, x_2), \cdots, k(x_{t+1}, x_t)] f_{t+1} \sim N(\mu_{t+1}, \sigma^2_{t+1})\ \mu_{t+1}(x_{t+1})$$

$$= k^T K^{-1} f_{1:t}\ \sigma^2_{t+1}(x_{t+1}) = k^T K^{-1} k + k(x_{t+1}, x_{t+1}) \quad (13)$$

The Gaussian model provides the probability distribution of each possible value of f_{t+1}. Thus, if enough sample point is gathered, then the Gaussian model is used for obtaining an approximate estimation of the objective function.

3.4.2 Acquisition Function

The sampling function guides the selection of the next sampling point in the decision space of the hyperparameter. The probability of improvement (PI) is utilized as a sampling function:

$$f(x) = \Phi\left(\frac{u(x) - f(x^+) - \xi}{\sigma(x)}\right) \quad (14)$$

In Eq. (14), $u(x)$, $\sigma(x)$ shows based on the Gaussian process and are the mean and variance of objective function values; ξ refers to the parameter. Φ denotes the cumulative density function of a standard distribution. $f(x^+)$ indicates the present optimum objective function value.

4. Results and Discussion

This section studies the performance of the ODCNN-ABTDC technique on two BT datasets namely BraTs-2019 and BraTs-2020 dataset. Table 1 represents the details of the BraTs-2019 dataset [22]. It has 670 samples with three classes.

Table 1. Details on BraTs-2019 dataset

Class	*No. of Images*
Glioma	335
HGG	259
LGG	76
Total Images	**670**

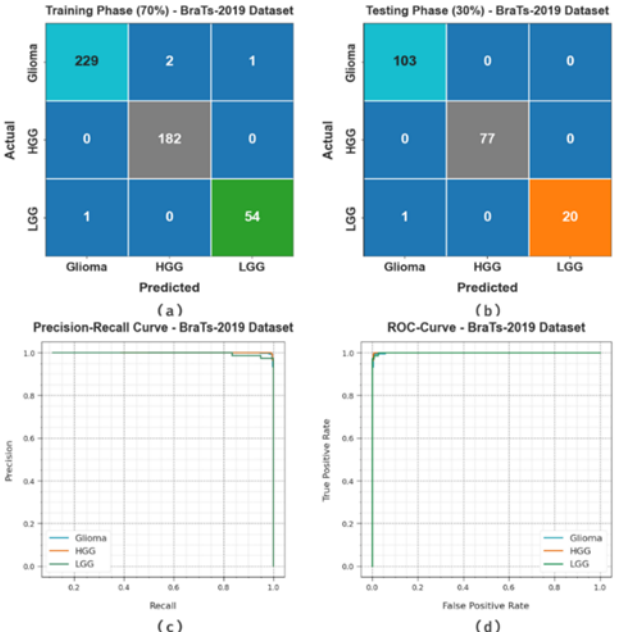

Fig. 3. BraTs-2019 dataset (a-b) Confusion matrices, (c) PR_curve, and (d) ROC

Fig. 3 illustrates s the classifier performances of the ODCNN-ABTDC algorithm on the BraTs-2019 database. Figs. 3a-3b defines the confusion matrices attained by the ODCNN-ABTDC approach on 70:30 of the TR set/TS set. The simulation outcome demonstrated that the ODCNN-ABTDC algorithm has detected

and classified all 3 classes accurately. Then, Fig. 3c exhibits the PR outcome of the ODCNN-ABTDC system. The simulation values that the ODCNN-ABTDC methodology has achieved greater values of PR on 3 classes. Moreover, Fig. 3d defines the ROC of the ODCNN-ABTDC algorithm. The outcome depicted that the ODCNN-ABTDC methodology led to capable performances with higher values of ROC on 3 classes.

Table 2 and Fig. 4 portray the BT detection result of the ODCNN-ABTDC methodology on the BraTs-2019 dataset. The outcome exhibits the effectual performance of the ODCNN-ABTDC technique on BT detection. With a 70% TR set, the ODCNN-ABTDC technique gains average $accu_y$, PPV, $sens_y$, $spec_y$, dice, and F_{score} values of 99.43%, 98.89%, 98.96%, 99.55%, 98.92%, and 98.90% respectively.

Table 2. BT detection outcome of ODCNN-ABTDC algorithm on BraTs-2019 dataset

Class	$Accu_y$	*PPV*	$Sens_y$	$Spec_y$	*Dice*	F_{score}
TR set (70%)						
Glioma	99.15	99.57	98.71	99.58	99.13	99.39
HGG	99.57	98.91	100	99.3	99.45	99.13
LGG	99.57	98.18	98.18	99.76	98.18	98.18
Average	**99.43**	**98.89**	**98.96**	**99.55**	**98.92**	**98.9**
TS set (30%)						
Glioma	99.5	99.04	100	98.98	99.52	99.23
HGG	100	100	100	100	100	100
LGG	99.5	100	95.24	100	97.56	99.01
Average	**99.67**	**99.68**	**98.41**	**99.66**	**99.03**	**99.41**

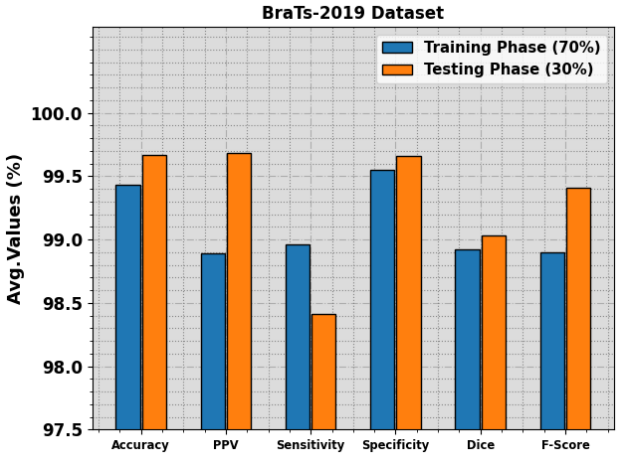

Fig. 4. Average of ODCNN-ABTDC algorithm on BraTs-2019 dataset

Additionally, with a 30% TS set, the ODCNN-ABTDC system achieves average $accu_y$, PPV, $sens_y$, $spec_y$, dice, and F_{score} values of 99.67%, 99.68%, 98.41%, 99.66%, 99.03%, and 99.41% correspondingly.

Fig. 5 represents the training accuracy TR_accu_y and VL_accu_y of the ODCNN-ABTDC system on the BraTs-2019 dataset. The TL_accu_y is defined by the estimation of the ODCNN-ABTDC system on the TR dataset whereas the VL_accu_y is computed by evaluating the performance on a separate testing dataset. The outcomes reveal that TR_accu_y and VL_accu_y increase with an upsurge in epochs. Accordingly, the performance of the ODCNN-ABTDC method gets improved on the TR and TS dataset with a rise in the number of epochs.

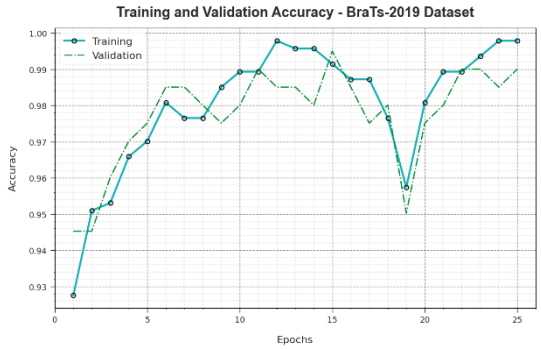

Fig. 5. $Accu_y$ curve of ODCNN-ABTDC algorithm on BraTs-2019 dataset

In Fig. 6, the TR_loss and VR_loss outcome of the ODCNN-ABTDC technique on the BraTs-2019 dataset is exposed. The TR_loss defines the error among the predictive solution and original values on the TR data. The VR_loss signifies the measure of the performance of the ODCNN-ABTDC technique on individual validation data. The results indicate that the TR_loss and VR_loss tend to be lesser with rising epochs. It represented the enhanced performance of the ODCNN-ABTDC technique and its capability to generate accurate classification. The lesser value of TR_loss and VR_loss determines the enhanced outcome of the ODCNN-ABTDC technique on capturing patterns and relationships.

Fig. 6. Loss curve of ODCNN-ABTDC algorithm on BraTs-2019 dataset

Table 3 demonstrates the details of the BraTs-2020 dataset [23]. It has 4575 samples with four classes.

Table 3. Details on BraTs-2020 dataset

Class	***No. of Images***
Normal	1500
Glioma	1427
Pituitary	940
Meningioma	708
Total Images	**4575**

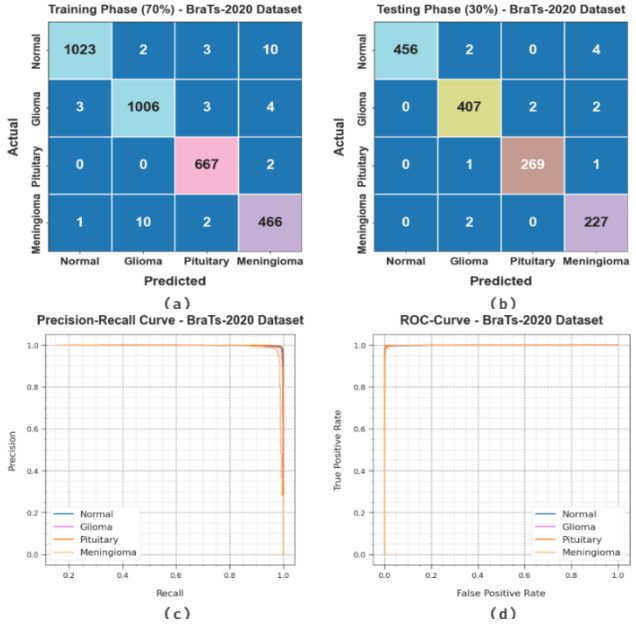

Fig. 7. BraTs-2020 dataset (a-b) Confusion matrices, (c) PR_curve, and (d) ROC

Fig. 7 defines the classifier outcome of the ODCNN-ABTDC methodology on the BraTs-2020 database. Figs. 7a-7b displays the confusion matrices achieved by the ODCNN-ABTDC algorithm on 70:30 of the TR set/TS set. The outcome depicted that the ODCNN-ABTDC system has detected and classified all 4 classes accurately. Afterwards, Fig. 7c represents the PR outcome of the ODCNN-ABTDC method. The simulation outcome is that the ODCNN-ABTDC algorithm has achieved greater values of PR on 4 classes. However, Fig. 7d defines the ROC outcome of the ODCNN-ABTDC algorithm. The simulation outcome demonstrates that the ODCNN-ABTDC methodology led to a capable outcome with superior values of ROC on 4 classes.

Table 4 and Fig. 8 represent the BT detection outcome of the ODCNN-ABTDC methodology on the BraTs-2020 dataset. The simulation value displays the effective performance of the ODCNN-ABTDC algorithm on BT detection.

With a 70% TR set, the ODCNN-ABTDC method reaches average $accu_y$, PPV, $sens_y$, $spec_y$, dice, and F_{score} values of 99.38%, 98.48%, 98.64%, 99.59%, 98.56%, and 98.51% correspondingly. Followed by, with 30% TS set, the ODCNN-ABTDC system gains average $accu_y$, PPV, $sens_y$, $spec_y$, dice, and F_{score} values of 99.49%, 98.76%, 99.03%, 99.67%, 98.89%, and 98.81% correspondingly.

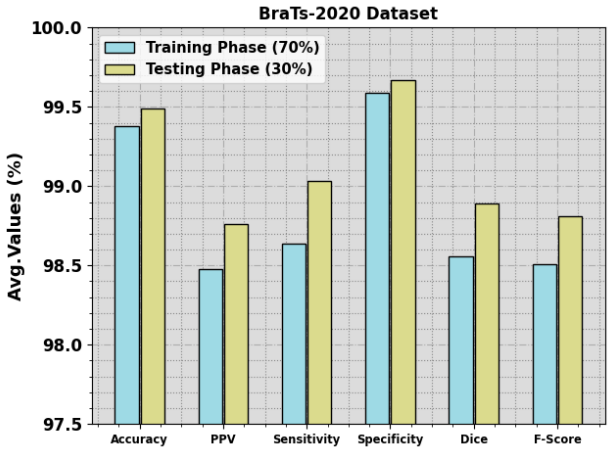

Fig. 8. Average of ODCNN-ABTDC algorithm on BraTs-2020 dataset

Fig. 9 defines the training accuracy TR_accu_y and VL_accu_y of the ODCNN-ABTDC system on the BraTs-2020 dataset. The TL_accu_y is determined by the assessment of the ODCNN-ABTDC method on the TR dataset whereas the VL_accu_y is calculated by evaluating the performance on a separate testing dataset. The outcomes display that TR_accu_y and VL_accu_y increase with an upsurge in epochs.

Table 4. BT detection outcome of ODCNN-ABTDC algorithm on BraTs-2020 dataset

Class	$Accu_y$	*PPV*	$Sens_y$	$Spec_y$	*Dice*	F_{Score}
TR set (70%)						
Normal	99.41	99.61	98.55	99.82	99.08	99.40
Glioma	99.31	98.82	99.02	99.45	98.92	98.86
Pituitary	99.69	98.81	99.70	99.68	99.26	98.99
Meningioma	99.09	96.68	97.29	99.41	96.98	96.80
Average	**99.38**	**98.48**	**98.64**	**99.59**	**98.56**	**98.51**
TS set (30%)						
Normal	99.56	100.00	98.70	100.00	99.35	99.74
Glioma	99.34	98.79	99.03	99.48	98.91	98.83
Pituitary	99.71	99.26	99.26	99.82	99.26	99.26
Meningioma	99.34	97.01	99.13	99.39	98.06	97.42
Average	**99.49**	**98.76**	**99.03**	**99.67**	**98.89**	**98.81**

Table 5. Comparative outcome of ODCNN-ABTDC algorithm with other approaches

Method	$Accu_y$	*PPV*	$Sens_y$	$Spec_y$	*Dice*	F_{Score}
CNN-SVM Model	95.83	93.64	92.22	92.43	90.06	91.43
Superv oxels-RF	80.00	92.84	89.19	93.96	91.29	94.65
Random Forest	80.85	93.56	89.52	93.27	94.83	91.31
Dual-Path Residual-CNN	84.90	94.52	92.29	93.97	90.22	89.38
Deep CNN-Data Augmentation	94.58	92.26	92.51	92.90	89.82	89.93
Multi-Layer Perceptron	94.12	93.67	95.81	94.41	93.49	94.04
ODCNN-ABTDC	99.67	99.68	98.41	99.66	99.03	99.41

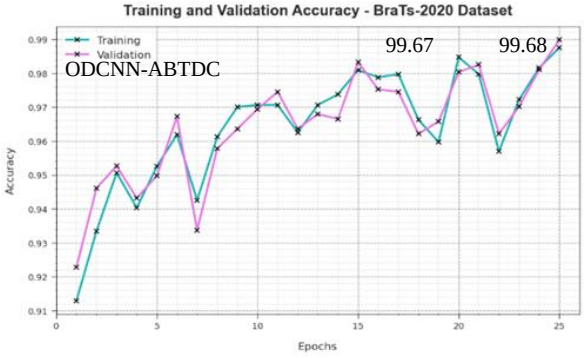

Fig. 9. $Accu_y$ curve of ODCNN-ABTDC algorithm on BraTs-2020 dataset

Consequently, the performance of the ODCNN-ABTDC system increases on the TR and TS datasets with a rise in the count of epochs.

In Fig. 10, the TR_loss and VR_loss outcome of the ODCNN-ABTDC technique on the BraTs-2020 dataset is exposed. The TR_loss defines the error among the predictive outcome and original values on the TR data. The VR_loss represents the measure of the solution of the ODCNN-ABTDC technique on individual validation data. The performance indicates that the TR_loss and VR_loss tend to decrease with rising epochs. It represented the enhanced performance of the ODCNN-ABTDC approach and its ability to produce accurate classification. The lesser value of TR_loss and VR_loss demonstrates the enhanced performance of the ODCNN-ABTDC technique in capturing patterns and relationships.

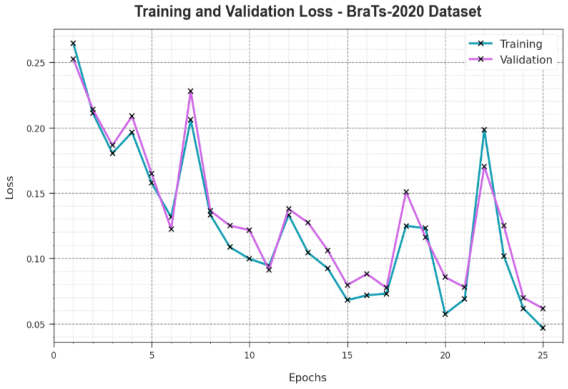

Fig. 10. Loss curve of ODCNN-ABTDC algorithm on BraTs-2020 dataset

The comparative results of the ODCNN-ABTDC technique on BT detection are demonstrated in Table 5 [24]. Fig. 11 examines the comparative outcome of the ODCNN-ABTDC system with respect to $accu_y$ and PPV. The results indicate the improved performance of the ODCNN-ABTDC technique. Based on $accu_y$, the ODCNN-ABTDC technique obtains an increased $accu_y$ of 99.67% while the CNN-SVM, S-RF, RF, DP RCNN, Deep CNN-DA, and MLP models offer decreased $accu_y$ of 95.83%, 80%, 80.85%, 84.90%, 94.58%, and 94.12% respectively. In the meantime, based on PPV, the ODCNN-ABTDC method achieves a higher PPV of 99.68%.

while the CNN-SVM, S-RF, RF, DP RCNN, Deep CNN-DA, and MLP systems offer a lesser PPV of 93.64%, 92.84%, 93.56%, 94.52%, 92.26%, and 93.67% correspondingly.

Fig. 12 demonstrates the comparative analysis of the ODCNN-ABTDC algorithm interms of $sens_y$ and $spec_y$. The outcome points out the better performance of the ODCNN-ABTDC method.

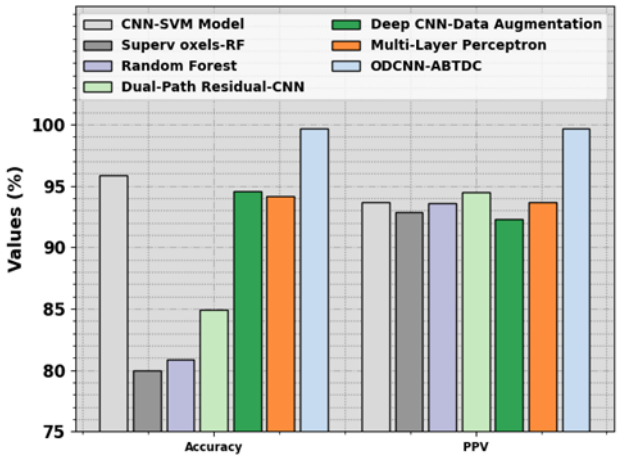

Fig. 11. $Accu_y$ and PPV outcome of ODCNN-ABTDC algorithm with other approaches

Based on $sens_y$, the ODCNN-ABTDC algorithm obtains enhanced $sens_y$ of 98.41% while the CNN-SVM, S-RF, RF, DP RCNN, Deep CNN-DA, and MLP algorithms offer minimal $sens_y$ of 92.22%, 89.19%, 89.52%, 92.29%, 92.51%, and 95.81% correspondingly. Afterwards, based on $spec_y$, the ODCNN-ABTDC algorithm gains maximal

$spec_y$ of 99.66% while the CNN-SVM, S-RF, RF, DP RCNN, Deep CNN-DA, and MLP approaches achieve lesser $spec_y$ of 92.43%, 93.96%, 93.27%, 93.97%, 92.90%, and 94.41% correspondingly.

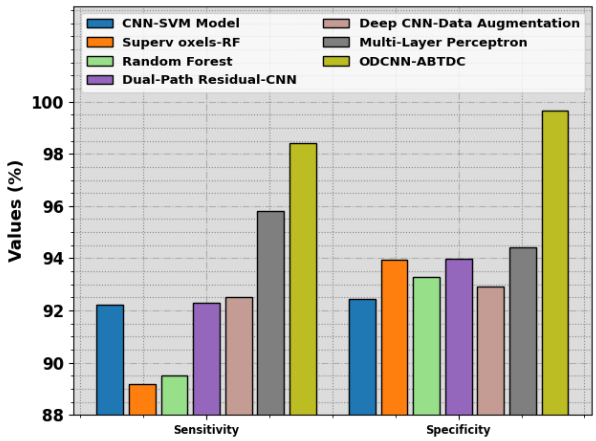

Fig. 12. $Sens_y$ and $spec_y$ outcome of ODCNN-ABTDC algorithm with other approaches

Fig. 13 illustrates the comparative study of the ODCNN-ABTDC approach with respect to Dice and F_{score}. The simulation value referred to the greater outcome of the ODCNN-ABTDC algorithm. Based on Dice, the ODCNN-ABTDC system achieves superior Dice of 99.03% while the CNN-SVM, S-RF, RF, DP RCNN, Deep CNN-DA, and MLP methods provide lesser Dice of 90.06%, 91.29%, 94.83%, 90.22%, 89.82%, and 93.49% respectively. Meanwhile, based on $the\ F_{score}$, the ODCNN-ABTDC approach reaches a higher F_{score} of 99.41% while the CNN-SVM, S-RF, RF, DP RCNN, Deep CNN-DA, and MLP methodologies achieve lesser F_{score} of 91.43%, 94.65%, 91.31%, 89.38%, 89.93%, and 94.04% correspondingly.

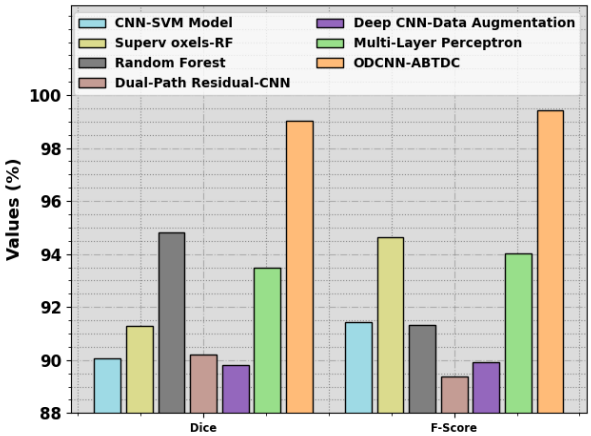

Fig. 13. Dice and F_{score} outcome of ODCNN-ABTDC algorithm with other approaches

These results confirmed the supremacy of the ODCNN-ABTDC technique in the BT detection process.

4. Conclusion

In this manuscript, we have offered the design and development of the ODCNN-ABTDC technique for the automated classification and detection of BT on MRI multi-modality Images. The ODCNN-ABTDC technique mainly focused on the examination of brain MRI images for the classification and recognition of BT. To accomplish this, the ODCNN-ABTDC technique involves several subprocesses namely preprocessing, GLCM feature extraction, CNN-based classification, and BO-based hyperparameter tuning. For the classification process, the ODCNN-ABTDC method employs the CNN model which allocates the images into proper classes. Finally, the performance of the CNN model can be boosted by the BO algorithm. The simulation value of the ODCNN-ABTDC algorithm is tested on the benchmark BRATS database. The extensive results demonstrated the greater solution of the ODCNN-ABTDC approach with other recent DL models**.**

References

[1] Demir, F., Akbulut, Y., Taşcı, B. and Demir, K., 2023. Improving brain tumor classification performance with an effective approach based on new deep learning model named 3ACL from 3D MRI data. Biomedical Signal Processing and Control, 81, p.104424.

[2] Srinivas, C., KS, N.P., Zakariah, M., Alothaibi, Y.A., Shaukat, K., Partibane, B. and Awal, H., 2022. Deep transfer learning approaches in performance analysis of brain tumor classification using MRI images. Journal of Healthcare Engineering, 2022.

[3] Bairagi, V.K., Gumaste, P.P., Rajput, S.H. and Chethan, K.S., 2023. Automatic brain tumor detection using CNN transfer learning approach. Medical & Biological Engineering & Computing, pp.1-16.

[4] Belfin, R.V., Anitha, J., Nainan, A. and Thomas, L., 2022. An Efficient Approach for Brain Tumor Detection Using Deep Learning Techniques. In International Conference on Innovative Computing and Communications: Proceedings of ICICC 2021, Volume 1 (pp. 297-312). Springer Singapore.

[5] Mahmud, M.I., Mamun, M. and Abdelgawad, A., 2023. A deep analysis of brain tumor detection from mr images using deep learning networks. Algorithms, 16(4), p.176.

[6] Nayan, A.A., Mozumder, A.N., Haque, M.R., Sifat, F.H., Mahmud, K.R., Azad, A.K.A. and Kibria, M.G., 2022. A deep learning approach for brain tumor detection using magnetic resonance imaging. arXiv preprint arXiv:2210.13882.

[7] Pedada, K.R., Rao, B., Patro, K.K., Allam, J.P., Jamjoom, M.M. and Samee, N.A., 2023. A novel

approach for brain tumour detection using deep learning based technique. Biomedical Signal Processing and Control, 82, p.104549.

[8] Obeidavi, M.R. and Maghooli, K., 2022, February. Tumor Detection in Brain MRI using Residual Convolutional Neural Networks. In 2022 International Conference on Machine Vision and Image Processing (MVIP) (pp. 1-5). IEEE.

[9] Rasheed, Z., Ma, Y.K., Ullah, I., Al Shloul, T., Tufail, A.B., Ghadi, Y.Y., Khan, M.Z. and Mohamed, H.G., 2023. Automated Classification of Brain Tumors from Magnetic Resonance Imaging Using Deep Learning. Brain Sciences, 13(4), p.602.

[10] Ghanshala, A., Chauhan, A., Diwakar, M. and Sharma, S., 2022, November. Brain Tumor Detection Using U-Net and 3D CNN Architecture. In 2022 International Conference on Computing, Communication, and Intelligent Systems (ICCCIS) (pp. 599-604). IEEE.

[11] Saeedi, S., Rezayi, S., Keshavarz, H. and R Niakan Kalhori, S., 2023. MRI-based brain tumor detection using convolutional deep learning methods and chosen machine learning techniques. BMC Medical Informatics and Decision Making, 23(1), pp.1-17.

[12] Vankdothu, R., Hameed, M.A. and Fatima, H., 2022. A brain tumor identification and classification using deep learning based on CNN-LSTM method. Computers and Electrical Engineering, 101, p.107960.

[13] Saurav, S., Sharma, A., Saini, R. and Singh, S., 2023. An attention-guided convolutional neural network for automated classification of brain tumor from MRI. Neural Computing and Applications, 35(3), pp.2541-2560.

[14] Dipu, N.M., Shohan, S.A. and Salam, K.A., 2021, August. Brain Tumor Detection Using Various Deep Learning Algorithms. In 2021 International Conference on Science & Contemporary Technologies (ICSCT) (pp. 1-6). IEEE.

[15] Alsubai, S., Khan, H.U., Alqahtani, A., Sha, M., Abbas, S. and Mohammad, U.G., 2022. Ensemble deep learning for brain tumor detection. Frontiers in Computational Neuroscience, 16, p.1005617.

[16] Harshavardhan, A., Maheswari, N.U., Prakash, M. and Sammeta, N., 2023, June. Deep Learning Algorithm for Brain Tumor Detection and Classification using MRI Images. In 2023 International Conference on Applied Intelligence and Sustainable Computing (ICAISC) (pp. 1-6). IEEE.

[17] Turk, O., Ozhan, D., Acar, E., Akinci, T.C. and Yilmaz, M., 2022. Automatic detection of brain tumors with the aid of ensemble deep learning architectures and class activation map indicators by employing magnetic resonance images. Zeitschrift für Medizinische Physik.

[18] Prakash, R.M., Kumari, R.S.S., Valarmathi, K. and Ramalakshmi, K., 2023. Classification of brain tumours from MR images with an enhanced deep learning approach using densely connected convolutional network. Computer Methods in Biomechanics and Biomedical Engineering: Imaging & Visualization, 11(2), pp.266-277.

[19] Zainal, Z., Ramli, R. and Mustafa, M.M., 2013. Grey-level cooccurrence matrix performance evaluation for heading angle estimation of moveable vision system in static environment. Journal of Sensors, 2013.

[20] Mali, S.D. and Agilandeeswari, L., 2023. Non-redundant shift-invariant complex wavelet transform and fractional gorilla troops optimization-based Deep Convolutional Neural Network for video watermarking. Journal of King Saud University-Computer and Information Sciences, p.101688.

[21] Du, Y., Xu, Z., Huang, J., Lyu, C., Lu, C. and Chen, J., 2023. Integrated Learning Activity Prediction Model of BHO-AdaBoosting Anti-Breast Cancer ERα Inhibitor Based on Improved Random Forest.

[22] https://opendatalab.com/BraTS-2019

[23] https://www.kaggle.com/datasets/awsaf49/brats2020-training-data

[24] Latif, G., Ben Brahim, G., Iskandar, D.A., Bashar, A. and Alghazo, J., 2022. Glioma Tumors' classification using deep-neural-network-based features with SVM classifier. Diagnostics, 12(4), p.1018.